Jin *et al. Advances in Bridge Engineering* (2022) 3:4
https://doi.org/10.1186/s43251-022-00055-0

Advances in
Bridge Engineering

ORIGINAL INNOVATION Open Access

Improving vehicle's seismic safety by equipping railway bridges with FPB and misalignment control device

Zhibin Jin*, Ke Chen and Jinzhe He

*Correspondence:
jinzhibin@swjtu.edu.cn

Department of Bridge Eng., Southwest Jiaotong University, Chengdu 610031, China

Abstract

Running safety of the railway vehicles on the bridge during earthquakes is a major concern for railway engineering. To reduce the derailment risk of railway vehicles on bridges, friction pendulum bearings (FPB) are proposed to be equipped on simply supported bridges in this study. The full nonlinear behavior of the FPB is introduced into the vehicle-bridge interaction model. The effect of FPB's manufacturing variations, including the shear pin's strength and friction coefficient, on the misalignment was investigated. The manufacturing variations of the FPB were found to produce large lateral misalignment, which further contributes to large wheel-rail forces when the vehicle passes over the girder ends. It diminishes the improvement in the vehicle's seismic safety provided by FPBs. Thus, a misalignment control device is proposed to limit the misalignment of the railway bridges equipped with FPBs. The vehicle-bridge interaction analysis results show that no wheel uplift occurred on the bridge equipped with FPBs and misalignment control devices during an earthquake. It indicates that the FPB significantly reduces the vehicle's derailment risk on bridges compared with the non-isolated bearings.

Keywords: Railway bridge, Friction pendulum bearing, Earthquake excitation, Railway vehicle, Running safety

1 Introduction

Rail transportation has developed rapidly worldwide in recent years. The high-speed railway network is expected to cover most areas of China by 2030 (Guo et al. 2020). A large portion of the railway line is supported by bridges, most of which are simply supported bridges. For instance, the bridge portions comprise more than 80% of the total railway mileage on the Beijing-Shanghai line. In earthquake-prone areas, the railway line is inevitable to cross the high seismic risk areas. Thus, there is a high probability that the train will run on the bridges when an earthquake occurs. The train derailed on the bridge during the Niigata earthquake of 2004, Tohoku earthquake of 2011, Kumamoto earthquake of 2016 (Japan Transport Safety Board et al. 2017), and Fukushima earthquake of 2022, which confirm these issues. Ensuring the running safety of the railway

vehicle over bridges during an earthquake has become a practical issue in the seismic design of railway networks.

After the Kobe earthquake and Niigata earthquake, the bridges on the Shinkansen railway in Japan were strengthened to improve the running quality of the vehicle subjected to earthquakes (Yoshida et al. 2010). Sogabe et al. (2007) also found that increasing the pier rigidity and damping can help to improve the running quality of the vehicles. However, increasing the bridge's seismic capacity and ductility means higher economic investments. An alternative solution for improving the bridge's performance under earthquake excitation is installing isolated bearings, which is an effective and inexpensive technique to reduce bridge damage.

The effect of friction pendulum bearing (FPB) on the seismic protection of bridges has been investigated extensively through analysis and experiments in previous studies. Tsopelas et al. (1996) experimentally studied the seismic performance of the bridge with FPB and a comparable non-isolated bridge. The experimental results showed that the FPB effectively reduced the bridge response, which was also confirmed by Madhekar and Jangid (2010). Yu et al. (2018) found that the FPB can effectively protect high-speed railway bridges and track structures. Hassan and Billah (2020) compared the seismic response of isolated bridges with three different isolation bearings. They found that the FPB showed promising performance in reducing residual isolator displacement. Fenz and Constantinou 2006; Mitoulis 2012; Eröz and DesRoches 2013; He et al. 2020 studied the influence of the pier height on the seismic isolation effectiveness of FPB for railway bridges. It was found that the seismic isolation ratios of the displacement and moment decrease with the increasing pier height when the pier height is more than 8 m. Jiang et al. (2019) proposed the appropriate strength of the double concave friction pendulum bearing's shear pin for railway bridges.

Most previous studies on isolated bearing focus on the bridge's seismic performance. Only a few studies have addressed the vehicle's safety on bridges installed with isolated bearings. Chen et al. (2019a) studied the running safety of the vehicles on isolated high-speed railway bridge subjected to near-fault earthquakes. The nonlinear hysteretic isolated bearing is idealized as a linear model through the equivalent linear method. Xiu Luo (2021) proposed a new type of seismic-isolated railway bridge to improve vehicle's seismic safety. Chen et al. (2019b) investigated the tuned mass damper (TMD) effect on the seismic vibration of the running vehicles. It was found that the attached TMD can reduce the amplitudes of the dynamic response of the vehicles.

In previous studies, all isolators' properties on the bridge are assumed to be identical. The variation of isolator properties due to manufacturing variations is not considered in the analysis of seismically isolated structures. In fact, the bearings may move at different paces since the variations in isolator properties (American Society of Civil Engineers 2016), leading to inconsistent deck motion (i.e., lateral misalignment). This lateral misalignment may increase the vehicle's derailment risk on the bridge (RTRI-Displacement Limits 2006). To reduce the derailment risk for the bridge with FPBs, a misalignment control device was proposed to limit the misalignment between two adjacent girders in the current study.

In this study, the full nonlinear behavior of the FPB was introduced into the vehicle-tack-bridge interaction model. The vehicle's performance on bridges equipped with

FPB was investigated, considering inconsistent deck motion (i.e., misalignment) caused by the variation of FPB product. The design requirement of the misalignment control device was proposed. The effect of the FPB with the misalignment control device on the vehicle's response was illustrated through incremental dynamic analysis.

2 Misalignment at girder ends caused by variations in FPB properties

The FPB was widely used in the seismic isolation design due to its high load and displacement capacity, well-set, stability and durability. The FPB prolongs the bridge's period through the motion of the superstructures on the curved surface. Thus, the natural period of the isolated bridge becomes independent of the mass of the superstructure. In addition, the friction force developed during the sliding motion provides energy dissipation, which reduces the lateral force and displacement (Eröz and DesRoches 2013).

The ASCE-7 2016 Standard has pointed out that the analysis of seismically isolated structures shall consider variations in seismic isolator properties. These include three categories: aging effect and environmental conditions, hysteretic heating and loading effects, and manufacturing variations. The standard also provides a systematic procedure for establishing isolator properties' upper and lower bound values (American Society of Civil Engineers 2016). The variations of isolator properties due to manufacturing may lead to an inconsistent bearing motion, and further contribute to a misalignment at the girder end, which adversely affects the seismic safety of the train on the bridges (RTRI-Displacement Limits 2006). In this section, the effect of the variations in FPB properties due to manufacturing on the misalignment was investigated.

2.1 Nonlinear behavior of FPB with shear pin

The FPB is simulated in the OpenSees platform using the *SingleFPBearing* element in this study. This element represents a curved surface slider with a single curved sliding surface. Under a constant axial load N and friction coefficient μ, the force–displacement behavior of the FPB in one horizontal direction is illustrated in Fig. 1b. The two parameters that govern performance are the characteristic strength Q_d at zero displacements and the post-elastic stiffness K_d. Q_d is related to the friction coefficient μ and the axial load N (i.e., $Q_d = \mu N$). K_d is related to the effective radius of curvature of the sliding surface R and the axial load N (i.e., $K_d = N/R$). Furthermore, the FPB has an initial stiffness $K_i$due to the shear deformation of the slider.

The seismic energy is dissipated by the friction action of the FPB, which is directly determined by the friction coefficient between the slider and curved surface. In this study, the friction behavior of the *SingleFPBearing* element is modeled as the Coulomb friction model with a constant friction coefficient μ and neglects the effects of sliding velocity, axial pressure, and heating of the curved surface.

The shear pins are installed on the FPBs to prevent them from sliding under service loads and small earthquakes (typically for PGA < 0.1 g). Under large earthquakes, the shear pins should fail to isolate seismic energy (Jiang et al. 2019). The shear pins are accounted for in the numerical formulation by introducing the Link element, which is parallel to the *SingleFPBearing* element and connected to the same nodes of the pier and the girder. The force–displacement behavior of the shear pin is modeled through the *MinMax* material object as an elastic uniaxial material, as shown in Fig. 1c. The shear

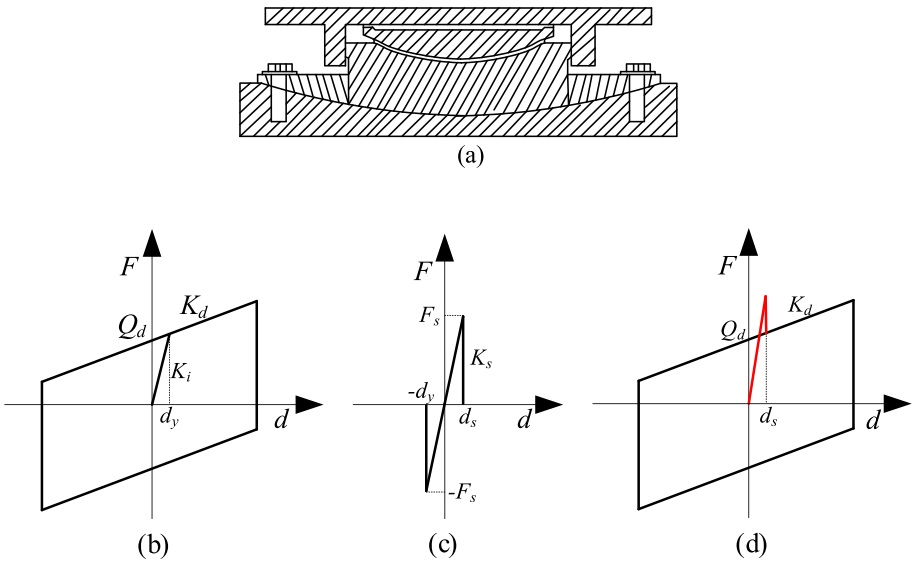

Fig. 1 Structure and force–displacement behavior of the FPB: **a** structure of FPB; **b** FPB model; **c** shear pin model; and **d** force–displacement behavior of FPB with the shear pin

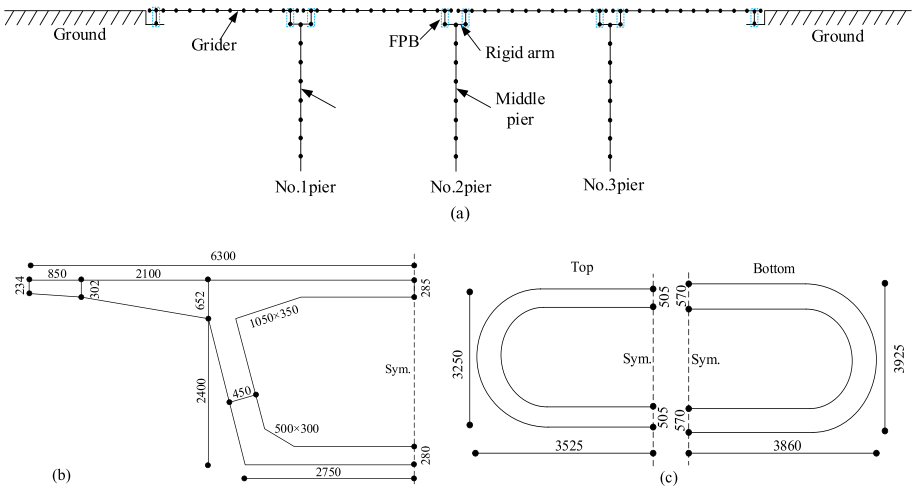

Fig. 2 Case bridge: **a** simply supported bridge; **b** girder section; and **c** pier section (unit in mm)

pin has a constant stiffness K_s (i.e., $K_s = F_s / d_s$) until the deformation achieves d_s, at which the material fails. Finally, the force–displacement behavior of the FPB with the shear pin is illustrated in Fig. 1d.

2.2 Case bridge

A case bridge in Fig. 2 was employed here to investigate the effect of variations in FPB properties on the misalignment. The track structure was not considered in this section to single out the primary sources of the misalignment. The box girder section and the hollow section of the piers were plotted in Fig. 2b and c, respectively, which were commonly used in the Chinese high-speed railway network. The pier height and span

Table 1 Nominal properties of the FPB

R/mm	N/kN	d_y/mm	μ	K_i/kN/mm	K_d/kN/mm	F_s/kN
2600	3196	2.5	0.06	76.7	1.23	508

length are 20 m and 32.6 m, respectively. The nominal properties of the FPB are listed in Table 1. In addition, the natural frequencies of the fundamental lateral and vertical modes were 2.50 Hz and 4.47 Hz, respectively.

2.3 Influence of variation in friction coefficient on the misalignment

As introduced earlier, the friction coefficient determines the characteristic strength and energy dissipation of the FPB, which significantly affects the bridge response. The nominal friction coefficient for analysis and design is taken as the average nominal value of the prototype isolators. Since the manufacturing variation, the friction coefficient of the FPBs on a bridge cannot be the same in actual engineering. The designer may adopt a ± 15% tolerance for manufacturing variations as recommended in ASCE 7–2016.

The variation in FPB's friction coefficient may affect the bridge's seismic response, especially for the deck motion of the adjacent girders. Since the friction forces and energy dissipation are different after the isolator slides, resulting in an inconsistent deck motion, which leads to a transverse misalignment at the girder ends. The misalignment adversely affects the running safety of the train (RTRI-Displacement Limits 2006).

To reveal the effect of variation of friction coefficient on the misalignments under seismic excitation. It is assumed that the friction coefficient has a normal distribution, and random friction coefficients are assigned to the isolators of the case bridge. The mean and standard deviation of the normal distribution are 0.06 (i.e., nominal value μ) and 0.003 (i.e., 0.05μ), respectively. In addition, the shear pin strength is 508kN (i.e., nominal value F_s). The ground motion recorded at Beverly Hills-14145Mulhol during the Northridge earthquake in 1994 was used as excitation, in which the peak ground acceleration (PGA) of the ground motion was 0.2 g. Figure 3 shows the absolute displacement responses of the girder ends, in which the displacement at an instant time (t = 12.45 s) is shown in Fig. 3b. There is a misalignment of 8 mm at No.2 pier due to manufacturing variation of the FPB's friction coefficient.

Random friction coefficients are assigned to the isolators of the case bridge; the maximum misalignment is obtained from the time history analysis under seismic excitation. The ground motion recorded at Beverly Hills-14145Mulhol during the Northridge earthquake in 1994 was used as excitation, in which the peak ground acceleration (PGA) of the ground motion was 0.2 g. Figure 4 illustrates the misalignment's distribution of 200 samples under seismic excitation. When the friction coefficient with a 15% tolerance for manufacturing variation, there is a maximum misalignment of 8 mm, which exceeds the minimum limit value of misalignment in a seismic condition (i.e., 6 mm) in the Japanese code (RTRI-Displacement Limits 2006). In addition, the distribution of the misalignment due to manufacturing variation is an asymmetric bimodal distribution, which has two clear peaks at near ± 3 mm.

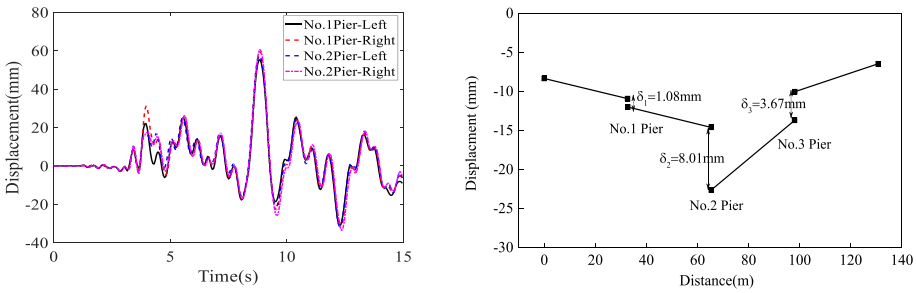

Fig. 3 Misalignment at girder end: **a** displacement response; and **b** misalignment

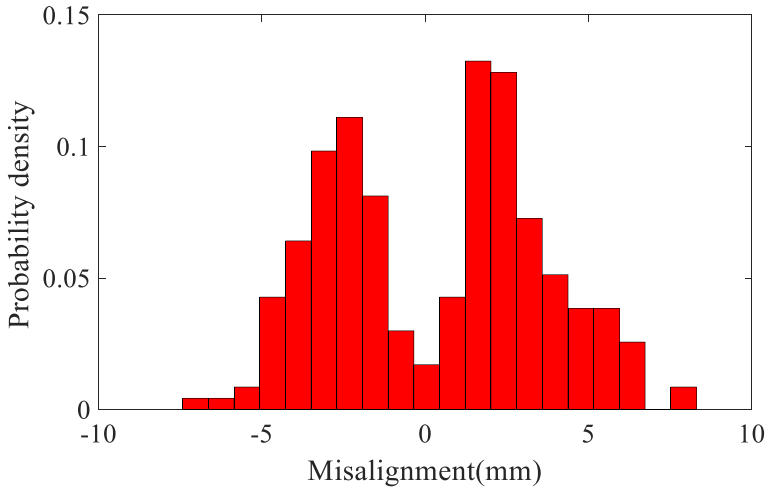

Fig. 4 Probabilistic relations between friction coefficient and misalignment

2.4 Influence of the variation in shear pin's strength on the misalignment

The shear pins are used to prevent FPB from sliding under service loads and small earthquakes, while the shear pins should fail to isolate seismic energy under large earthquakes. The shear pin's strength determines the cut-off time of the FPB, which affects the seismic response of the bridge deck. Due to the manufacturing variations, the cut-off time of the FPBs cannot be the same, resulting in an inconsistent deck motion and leading to a transverse misalignment at the girder ends.

Random strengths with normal distribution were assigned to the case bridge's FPBs in Fig. 2. The mean and standard deviation of the shear pin's strength is 508 (i.e., nominal value F_s) and 25.4 (i.e., $0.05F_s$), respectively. The friction coefficient is 0.06. In addition, the peak ground acceleration of the ground motion was 0.2 g. Figure 5 shows the distribution of the misalignment under seismic excitation. There is a maximum misalignment of 12 mm when the strength with a 15% tolerance for manufacturing variation. In addition, it is evident that the distribution of the misalignment caused by the variation in the shear pin's strength approaches a discrete distribution. This distribution with clear peaks at 0 mm and 10 mm. However, there is a gap between 5 and 10 mm.

The time history of the shear pin's shear force can explain the gap in the misalignment between 5 and 10 mm in Fig. 5. Assuming the shear pin has infinite strength,

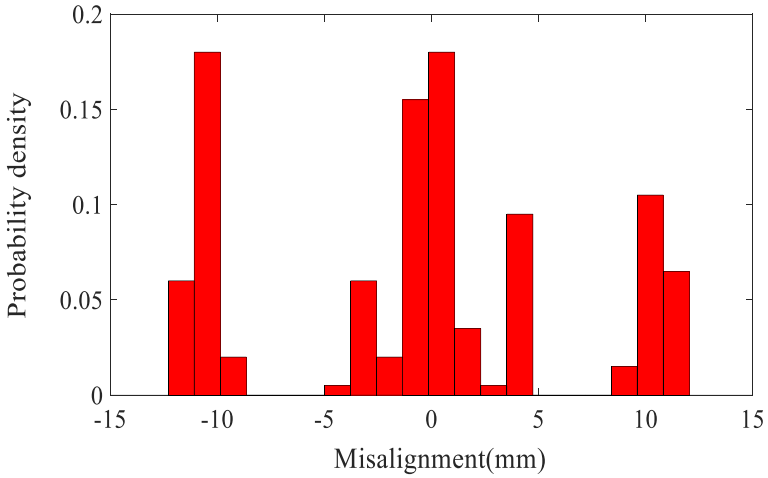

Fig. 5 Probabilistic relations between shear pin's strength and misalignment

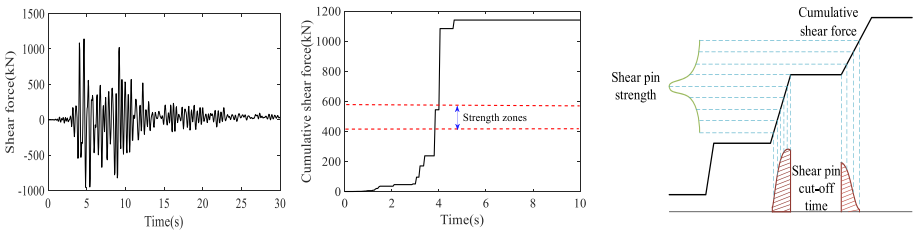

Fig. 6 The relations between cumulative shear force and cut-off time: **a** shear force; **b** cumulative shear force; and **c** cut-off time

i.e., the shear pin will not fail. Figure 6a shows the time history of the shear pin's shear force *f* under seismic excitation. The maximum shear force before instant *t* can be obtained as follow:

$$F(t) = \max\left(\left|f(\tau)\right|\right)\tau \le t \tag{1}$$

Figure 6b shows the maximum shear force of the shear pin before instant *t*. The horizontal segment of *F(t)* means that the shear pin's shear force in the time duration of the segment does not exceed the maximum shear force at the beginning of this segment. Therefore, if the shear pin is not cut off at the beginning of this segment, it will not be cut off during the duration of this horizontal segment. In other words, the shear pin will only be cut off during the slope segment of the *F(t)* function (seen in Fig. 6c). If the shear pins of the adjacent FPBs are cut off at the same slope segment of the *F(t)* function, then it will cause a slight misalignment at the girder ends. Otherwise, a large misalignment will be caused when the shear pins are cut off at the different slope segments. The shear pin will not be cut off at the horizontal segment in Fig. 6b, leading to a gap between 5 and 10 mm in the misalignment distribution.

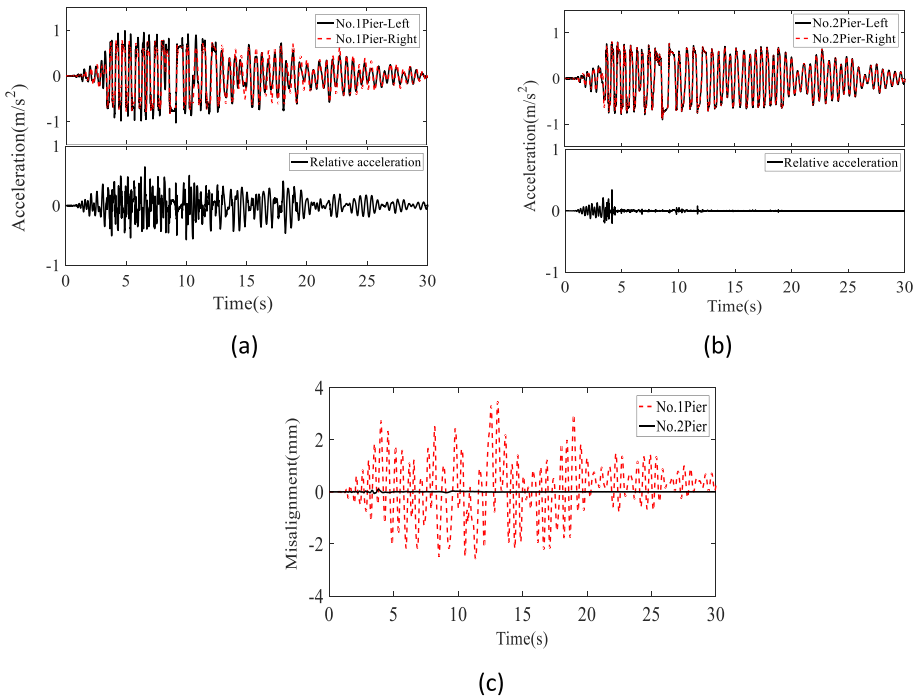

Fig. 7 Misalignment caused by an asymmetric boundary condition: **a** acceleration of girder on No.1 pier; **b** acceleration of girder on No.2 pier; and **c** misalignment

2.5 Influence of asymmetric boundary condition on the misalignment

The asymmetry boundary condition of the bridge is provided by the supported condition of the bearings on either side of the piers, which are affected by the number of spans, span length, and pier height. It can lead to different seismic loads in FPBs, resulting in the potentially inconsistent shear pin's cut-off time. Only the asymmetry boundary condition provided by the number of spans was considered in this study. The case bridge in Fig. 2 was used to investigate the effect of asymmetric boundary conditions on the misalignment. The acceleration response and misalignments of No.1 pier and No.2 pier under earthquake excitation with a PGA of 0.2 g are displayed in Fig. 7.

It can be seen from Fig. 7c that, there is a 3.5 mm misalignment at the girder end on the No.1 pier with asymmetric boundary conditions. The reason is that the acceleration responses of adjacent girders on the No.1 pier are different (see Fig. 7a), leading to an inconsistent shear pin's cut-off time of the adjacent FPBs and a significant misalignment occurs. On the contrary, the misalignment on the No.2 pier with symmetrical boundary is nearly zero since this pier is on the symmetric line of the whole bridge.

3 Effect of track constraint and misalignment control device on the misalignment

According to the previous calculation and analysis, the variations in FPB's properties and asymmetric boundary conditions can lead to a large misalignment at girder ends under seismic excitation. Nevertheless, the actual railway bridges are connected by track structure; the continuous track running across all bridge spans may reduce the misalignment.

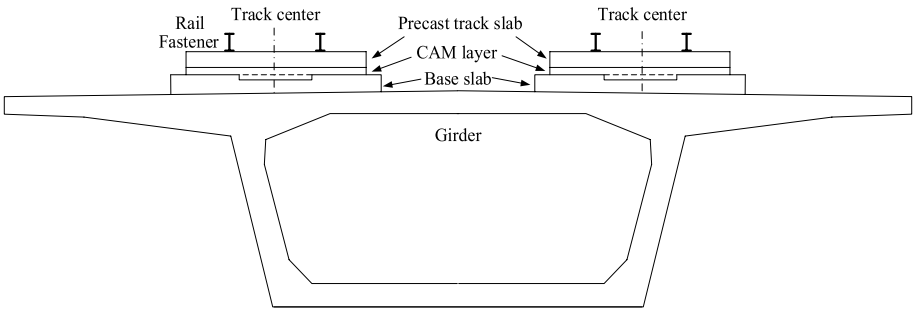

Fig. 8 Cross-section of the double-track railway bridge

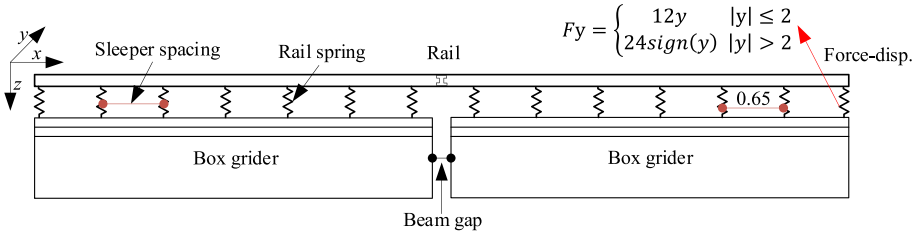

Fig. 9 Beam model with discrete point supports

In this section, a 50-span simply supported bridge is established to determine the effect of track constraint and misalignment control device on the misalignment at the girder end.

3.1 Track constraint on the bridge deck

China Railway Track System (CRTS) III type ballastless slab track structure is commonly applied on Chinese high-speed railway bridges. This track system consists of the base slab, precast track slab, rail, and fasteners, as shown in Fig. 8. The base slab is fixed on the bridge deck since their concrete is poured together and will not be separated. The precast concrete slabs are connected to the base slab by a cement asphalt mortar (CAM) layer. Also, the lateral stopper limits the transverse displacement of the precast concrete slab. The base slab and precast concrete slab break at the girder end between adjacent girders. Therefore, the adjacent girders are only constrained by the continuous rail-fastener system.

The rail-fastener system is modeled as a beam model with discrete point supports (Zhai 2020), as shown in Fig. 9. In this study, the continuous rail beam adopts the CN60 rail, which was commonly used in the Chinese high-speed railway network. The bending moment of inertia about the rail section's lateral axis and the vertical axis is 3.217×10^{-5} m^4 and 5.24×10^{-6} m^4, respectively. The elastic modulus of rail is 2.059×10^{11} N/m^2. The fastener system is modeled as a nonlinear spring (Bin et al. 2016), and the lateral force–displacement relationship is shown in Fig. 9. In addition, the sleeper spacing is 0.65 m. In this way, the shear force of the track system at the girder ends can be obtained by increasing the relative lateral displacement at the girder end.

Figure 10 shows the force–displacement behavior of the track constraint at the girder end obtained by the beam model with discrete point support. The force–displacement

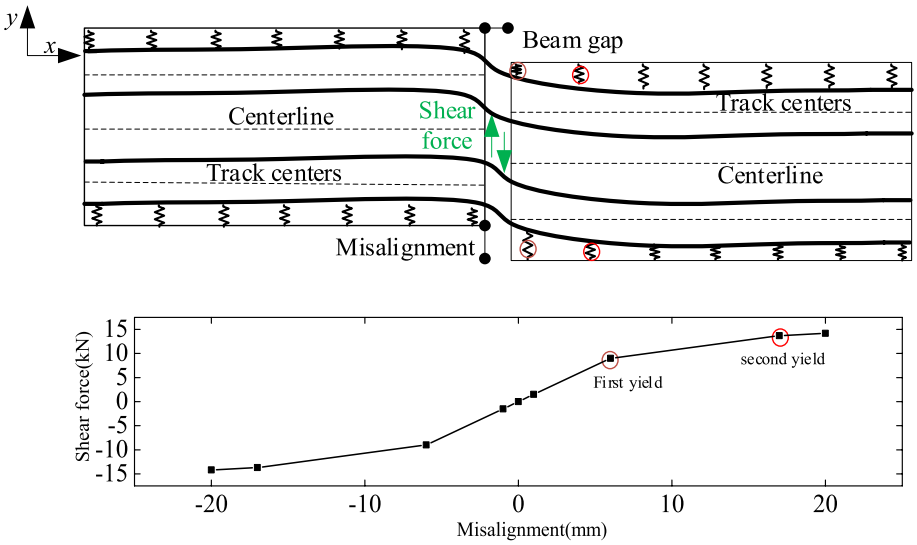

Fig. 10 Fore-displacement behavior of the track constraint at girder ends

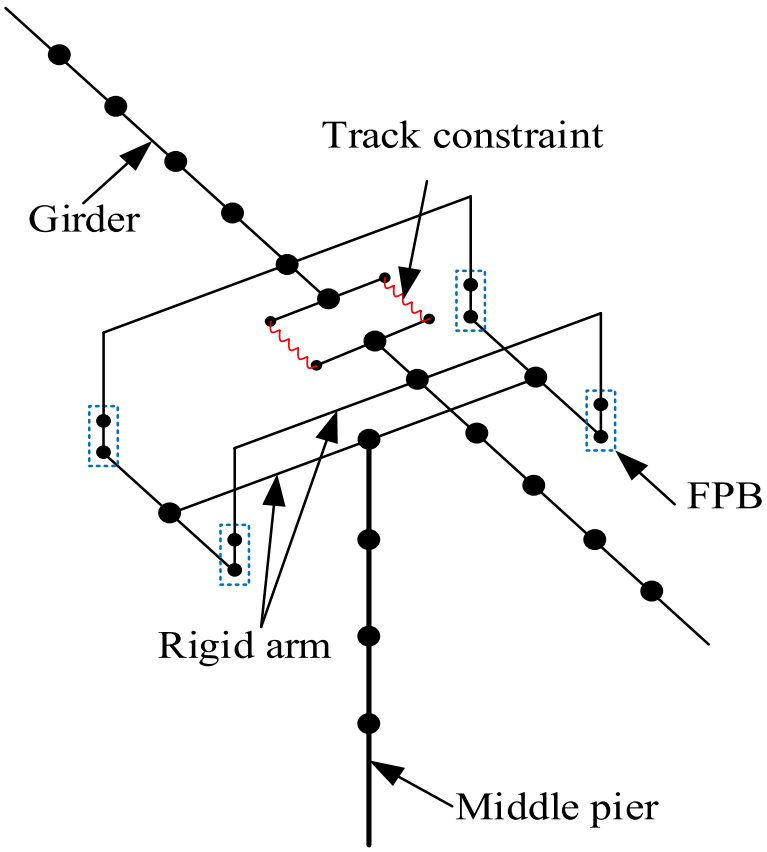

Fig. 11 Bridge model with track constraint

behavior of the fastener is bilinear. Thus, the force–displacement behavior of the track constraint at the girder end is multi-linear since the fasteners yield one by one as the misalignment increases. Meanwhile, in the following analysis, the track constraint is modeled as a nonlinear element at girder ends, as shown in Fig. 11.

3.2 Influence of track constraint on the misalignment

A 50-span simply supported girder bridge is used to investigate the effect of track constraint on misalignment at the girder ends. The box girder section and the hollow section of the piers were plotted in Fig. 2. The height of the piers is 20 m. The fundamental natural modes in the lateral and vertical directions are shown in Fig. 12; the corresponding natural frequencies of the fundamental lateral and vertical modes are 2.37 Hz and 4.45 Hz, respectively. In this section, the shear pin's strength and friction coefficient were assumed to obey normal distribution, and the strength and friction coefficient with a 15% tolerance for manufacturing variation. Random friction coefficients and shear pin's strength are assigned to the FPB of the bridge; the strength and friction coefficient of all the FPBs are plotted in Fig. 13.

Two scenarios are formulated to study the effect of track constraints on misalignment. Case 1 does not consider track constraint; Case 2 considers the normal track constraint. Figure 13c shows the maximum misalignment at girder ends for different scenarios under earthquake excitation with a PGA of 0.2 g. It can be seen from Fig. 13 that the normal track constraint moderately reduces the amplitudes of the misalignment under seismic effects. However, the maximum misalignment exceeds the minimum limit value of misalignment in a seismic condition (i.e., 6 mm) in the Japanese code (RTRI-Displacement Limits 2006), which adversely affects the running safety of the train on the bridges.

3.3 Misalignment control device

As introduced earlier, the track system can provide lateral constraints for the adjacent girders. However, the maximum misalignment will exceed the minimum limit value of misalignment in a seismic condition. Thus, the following device in Fig. 14 is proposed to limit the misalignment at the girder ends. This device consists of the base plate, ribbed plate, and fixed pin roller. The base plate has a linear slot at its end, and the slot length is larger than the beam gap (typically, a simply supported bridge is 0.1 m). The base plate and the pin roller are installed at the bottom of the adjacent girders, respectively, and

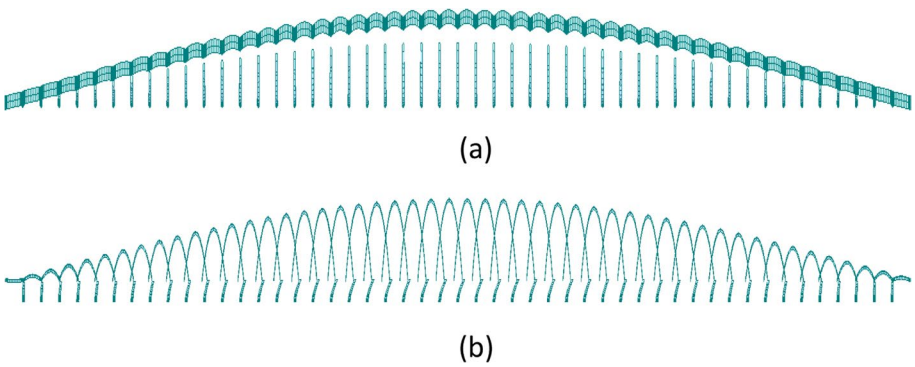

Fig. 12 Fundamental natural modes: **a** lateral mode; and **b** vertical mode

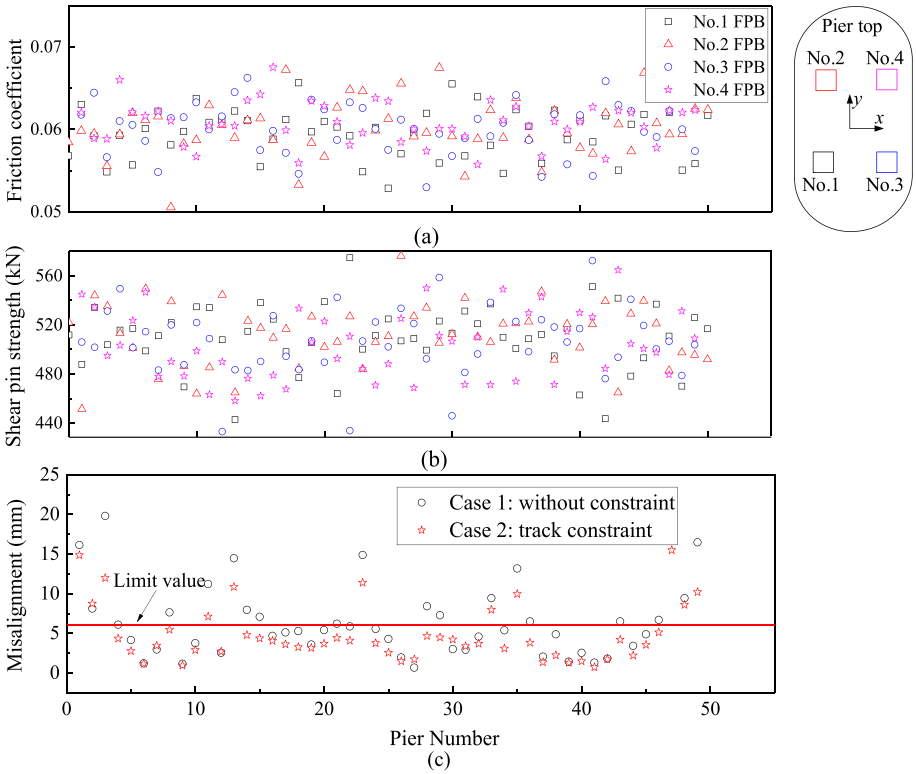

Fig. 13 FPB properties and maximum misalignment: **a** friction coefficient; **b** strength; and **c** misalignment

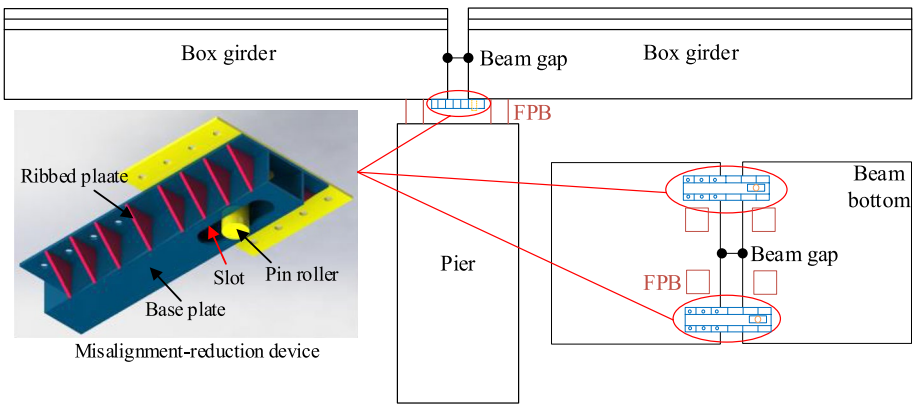

Fig. 14 Proposed misalignment control device

two devices are installed on adjacent girders. The working mechanism of the device is similar to that of a pin-slot joint. The relative rotation and longitudinal motion between the adjacent girders are not constrained, while the relative lateral motion is constrained. In this way, the misalignment caused by the variations of FPB properties can be significantly reduced.

The minimum strength of the device is determined by the manufacturing variation of the FPB. A ± 15% tolerance for manufacturing variations as recommended in ASCE 7–2016. Thus, the minimum strength of the device should be larger than 0.3 times the nominal strength of the shear pin (i.e., 152kN). In addition, the minimum limit value of

misalignment in a seismic condition is 6 mm in the Japanese code (RTRI-Displacement Limits 2006). The minimum lateral stiffness of the device can be determined as follow:

$$K_{md} = \frac{F_{md}}{\delta_L n} \tag{2}$$

where F_{md} denotes the device's strength, δ_L denotes the limit value of misalignment in a seismic condition, n denotes the number of devices installed on adjacent girders, and $n=2$ in this study. Therefore, the lateral stiffness of the device is set as 12.7kN/mm in this study. Meanwhile, this device is modeled as a linear element added in Fig. 11.

Case 3 is formulated to study the effect of the misalignment control device on the misalignment. The device is modeled as a linear element with its lateral stiffness of 12.7kN/mm added in Fig. 11. The strength and friction coefficient of all the FPBs are the same as Case 2, as shown in Fig. 13. Figure 15 shows the maximum misalignment of the bridge under seismic excitation, in which the PGA is 0.2 g. It is evident that the misalignment control device can effectively limit the misalignment caused by manufacturing variation of FPB and asymmetric boundary conditions. The maximum misalignment of Case 3 is 4.7 mm, which is smaller than the minimum limit value (i.e., 6 mm), indicating that this device can improve the vehicle's seismic safety on the bridge with FPBs.

4 Vehicle-track-bridge interaction model

The dynamic interaction model of the vehicle-track-bridge system in Jin et al. (Jin and Pei 2016) is adopted. The full nonlinear behavior of the FPB was introduced to the vehicle-tack-bridge interaction model in Jin et al. (Jin and Pei 2016).

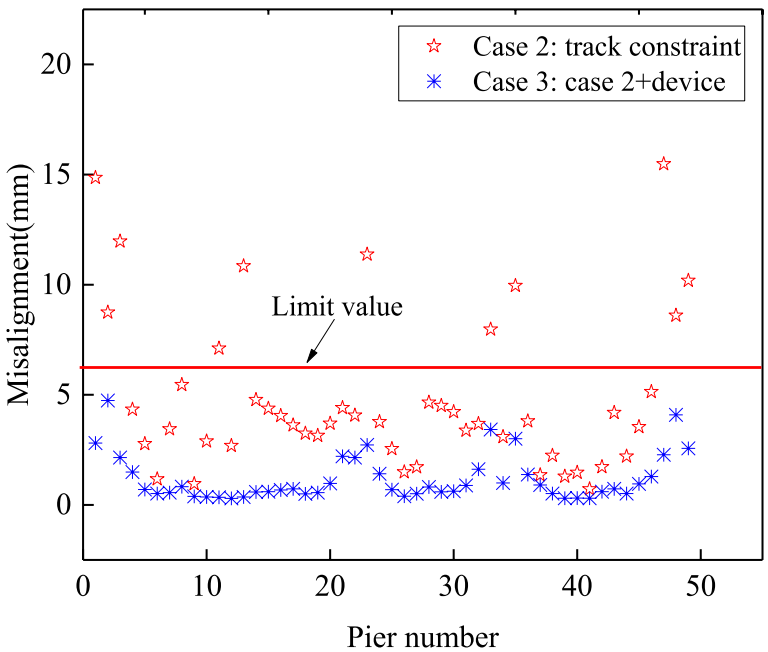

Fig. 15 Maximum misalignment under seismic excitation

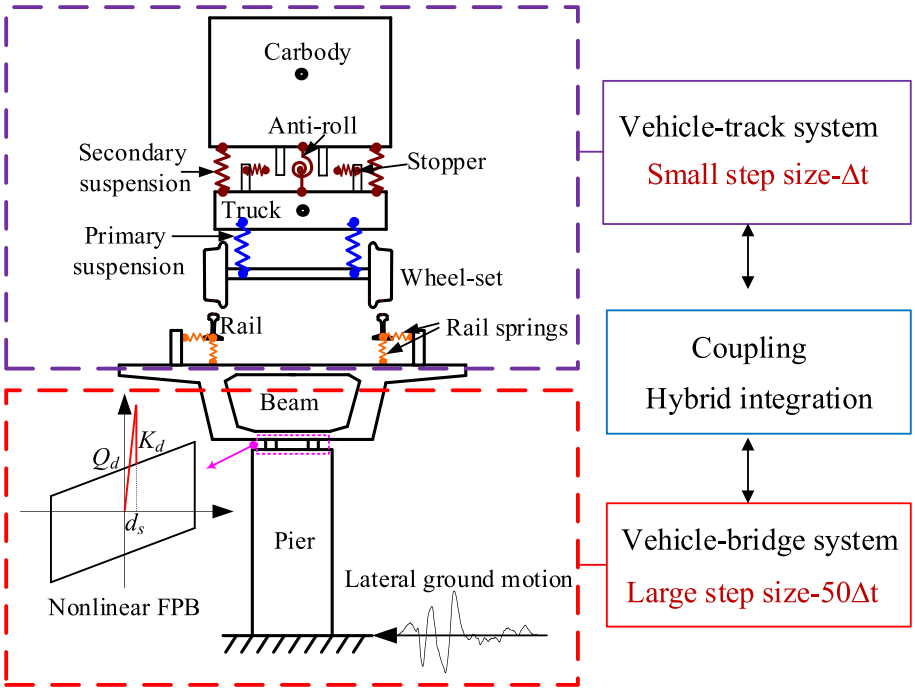

Fig. 16 vehicle-track-bridge dynamic interaction model

This coupled model involves three sub-systems of vehicle, track, and bridge, spatially coupled by wheel-rail and track-bridge interactions, as shown in Fig. 16. The vehicle-track and track-bridge simulation programs are developed on the C++and OpenSees platforms, respectively. Furthermore, the two platforms communicate through the Cython package to simulate the dynamic interaction between the vehicle and the bridge.

4.1 Vehicle-track model

The train is idealized as seven rigid bodies of a car-body, two trucks, and four wheelsets. The train is assumed to move along the track at a constant speed. The design speed of the train used in this study is 200 km/h. Therefore, the car-body and truck have five DOFs, i.e., lateral, vertical, roll, yaw, and pitch motions. The wheelset rotates at a constant rotational speed, so the pitch motion of the wheelset is neglected, i.e., each wheelset has four DOFs. As a result, the vehicle sub-system has 31 DOFs. The dynamic equation of the vehicle system can be written as

$$M_V \ddot{Y}_V + C_V \dot{Y}_V + K_V Y_V = F_V^r - F_V^g \tag{3}$$

where M_v, C_v, and K_v denote the mass, damping, and stiffness matrix of the vehicle system; Y_V, $\dot{Y}_V$, and $\ddot{Y}_V$ denote the displacement, velocity, and acceleration vectors; F_V^r denotes the force vector acting on the vehicle from the rail, which can be calculated in each integration step; F_V^g denotes the seismic force applied on the vehicle.

The rail structure beneath each wheel is idealized as a two DOFs oscillator (i.e., lateral and vertical motion). The mode shape of the rail was approximated by the static

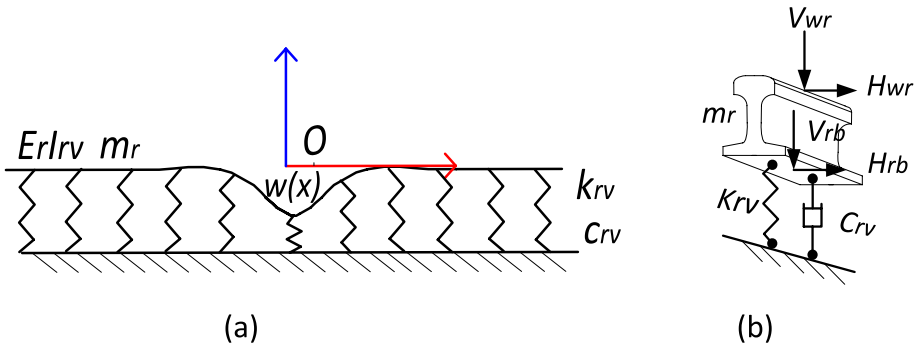

Fig. 17 Moving rail method (Jin and Pei 2016): **a** shape function of the rail; and **b** Moving rail model

deformation of the rail due to a stationary force (seen in Fig. 17). The mass, stiffness, and damping of the vertical motion can be obtained as follow

$$M_{rv} = m_r \int_{-\infty}^{\infty} w(x)dx \tag{4}$$

$$K_{rv} = k_{rv} \int_{-\infty}^{\infty} w^2(x)dx + E_r I_{rv} \int_{-\infty}^{\infty} [\frac{dw^2(x)}{dx^2}]dx \tag{5}$$

$$C_{rv} = c_{rv} \int_{-\infty}^{\infty} w(x)dx \tag{6}$$

where w(x) is the shape function of the rail, which can be obtained in Jin et al. (Jin and Pei 2016), m_r is the mass of the rail per unit length, k_{rv} and c_{rv} are the vertical stiffness and damping of the supporting pad under the rail per unit length, respectively, E_r is the elasticity modulus of the rail and I_{rv} is the bending moment of inertia about the lateral axis of the rail section. The lateral motion's mass, stiffness, and damping can be derived parallel with the vertical motion.

The dynamic equation of the rail can be written as.

$$M_r \ddot{Y}_r + C_r \dot{Y}_r + K_r Y_r = F_r^w + F_r^b - F_r^g \tag{7}$$

where M_r, C_r, and K_r denote the mass, damping, and stiffness matrix of the rail, respectively; Y_r, $\dot{Y}_r$, and $\ddot{Y}_r$ denote the displacement, velocity, and acceleration vectors, respectively; F_r^w and F_r^b denote the force vector acting on the rail from the wheel and bridge deck, respectively; F_r^g denote the seismic force acting on the rail.

4.2 Bridge model

The bridge is established through the finite element method (FEM). The bridge structure is simulated as 3D beam elements, and each node has six DOFs. The damping matrix C_b is assumed to be of the Rayleigh type and the damping ratio is 0.05. The full nonlinear model of the FPB in the OpenSees platform is considered in the bridge system. The force–displacement behavior of this FPB model is shown in Fig. 1. The track constraint is

modeled as a nonlinear element whose force–displacement behavior is shown in Fig. 10. In addition, the misalignment control device is modeled as a linear element (seen in Fig. 12). The dynamic equation of the bridge system can be written as

$$M_b\ddot{u}_b + C_b\dot{u}_b + K_b u_b = F_b^r - F_b^g \tag{8}$$

where M_b, C_b, and K_b denote the mass, damping, and stiffness matrices of the bridge, respectively; u_b, $\dot{u}_b$, and $\ddot{u}_b$ denote the displacement, velocity, and acceleration vectors, respectively; F_b^r denotes the force between the bridge and the track; F_b^g denotes the seismic force acting on the bridge.

4.3 Wheel-rail contact model and numerical algorithms

Under earthquake conditions, the extensive interaction between the wheel and rail could lead to wheel-rail separation and strong impact, so a nonlinear wheel-rail coupling model is adopted here. This model uses the trace curve method to solve the wheel-rail contact geometry relationship (Zhai et al. 2013). The wheel-rail normal contact forces are derived by nonlinear Hertzian elastic contact theory (Zhai et al. 2013). In addition, the tangent wheel-rail creep forces are calculated by Shen-Hedrick- Elkins nonlinear model (Shen et al. 1983).

An integrated explicit–implicit algorithm is adopted in this study to improve the computational efficiency (Jin et al. 2018). The Newmark/ Newton–Raphson method is selected to solve the nonlinear response of the bridge-track system with a large step size. On the other hand, Zhai's method is adopted to solve the vehicle-track subdomain with a small step size. In this study, a small step size Δt, is set to be 0.0001 s, and the large step size is 50Δt, i.e., 0.005 s.

5 Effect of the FPB on the running safety of the vehicles on bridges during earthquakes

Previous investigations have shown that the FPB effectively reduces the bridge's seismic response by prolonging its fundamental period. Nevertheless, for the whole railway system, the primary goal of the FPB is to reduce the seismic responses of the bridge structure, such as pier shear force and base moment. The effect of the FPB on the vehicle's seismic safety is not clear enough. Thus, it is necessary to figure out the influences of the FPB on the vehicle's safety over the bridge during an earthquake.

5.1 Bridge scenario

A large portion of the railway line is supported by bridges, most of which are simply supported bridges. Thus, the simply supported bridge was adopted here to investigate the vehicle's seismic safety on the bridge with FPBs. The box girder section and the hollow section of the piers were plotted in Fig. 2b and c, respectively. The pier height and span length are 20 m and 32.6 m, respectively. In addition, the number of bridge spans is set as 50, making the train on the bridge when peak acceleration attacks the bridge and the train passes over the beam gap. The natural frequencies of the fundamental lateral and vertical modes were 2.37 Hz and 4.45 Hz, respectively.

Table 2 Ground motion records

ID Number	Name	Magnitude	Recording station	PGA/g
1	Northridge	6.7	Beverly Hills-14145 Mulhol	0.52
2	Northridge	6.7	Canyon Country-W Lost Cany	0.48
3	Duzce, Turkey	7.1	Bolu	0.82
4	Hector Mine	7.1	Hector	0.34
5	Imperial Valley	6.5	Delta	0.35
6	Imperial Valley	6.5	El Centro Array #11	0.38
7	Kobe, Japan	6.9	Nishi-Akashi	0.51
8	Kobe, Japan	6.9	Shin-Osaka	0.24
9	Kocaeli, Turkey	7.5	Duzce	0.36
10	Landers	7.3	Yermo Fire Station	0.24
11	Landers	7.3	Coolwater	0.42

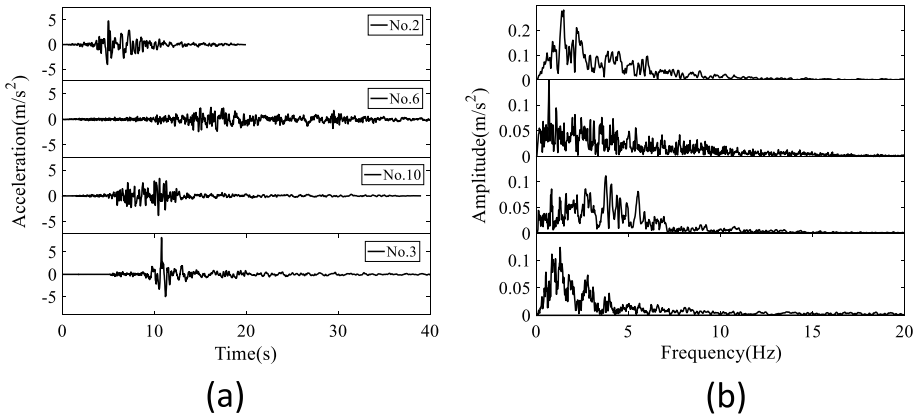

Fig. 18 Ground motion records: **a** time-domain; and **b** frequency-domain

5.2 Ground motion

Eleven different actual ground motion records suggested in FEMA P695 (Federal Emergency Management Agency 2009) were selected as inputs to the vehicle-track-bridge system. Their name, magnitudes, recording stations, and PGA are listed in Table 2. Figure 18 illustrates the accelerations and frequency spectra of Nos.2, 3, 6, and 10 ground motions. The figure shows that the amplitudes of these ground motions vary from 0.24 g to 0.82 g, and the dominant frequencies of these ground motions are different.

5.3 Effect of the misalignment on wheel-rail forces

For different FPB properties and constraint conditions, three scenarios are included to determine the misalignment's influence on wheel-rail forces during an earthquake. Case 4 assumes perfect FPBs, i.e., all bearings are identical. The normal track constraint is also considered in Case 4; Case 5 considers the FPB's manufacturing variation and normal track constraint; Case 6 further considers the misalignment control device based on Case 5. The random friction coefficient and strength were assigned to the isolators of the bridge. Figure 13 shows all the FPB properties in Case 5 and Case 6.

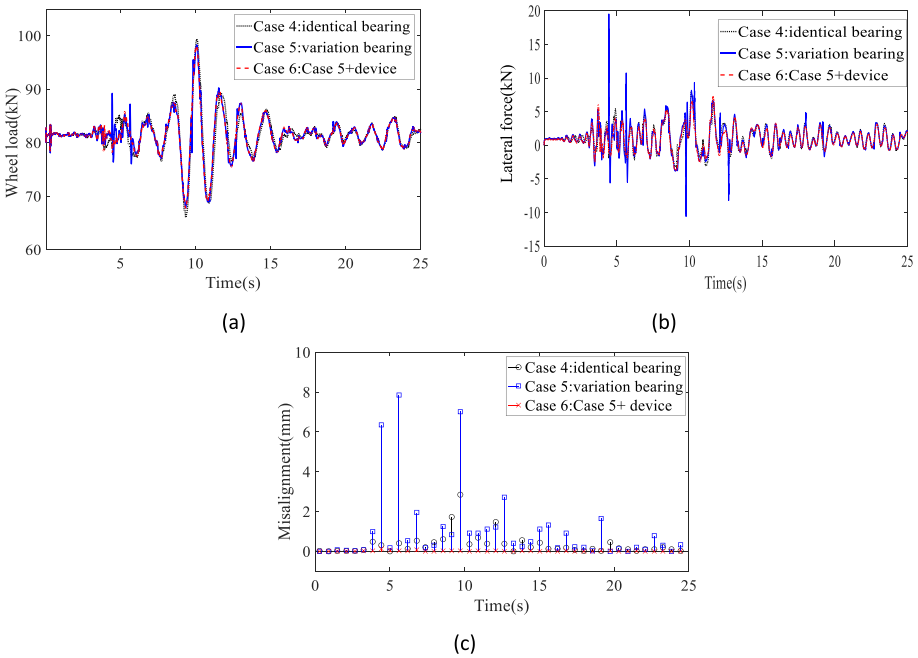

Fig. 19 Wheel-rail forces for No.1 ground motion input: **a** wheel load; **b** lateral wheel-rail force; and **c** maximum misalignment beneath wheel

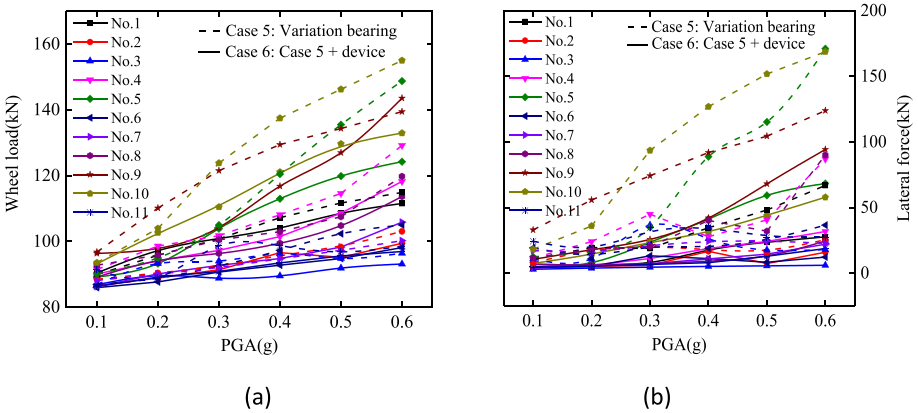

Fig. 20 IDA results of wheel-rail force with different constraint conditions: **a** wheel load; and **b** lateral force

Figure 19 illustrates the influences of the misalignment on the wheel-rail force. In this simulation, the vehicle speed is 200 km/h, and the PGA of the No.1 ground motion is 0.2 g. Because the manufacturing variation of the FPB results in a misalignment at the girder ends, the vehicle is subject to a significant lateral impact when the wheelsets pass the girder end. It can be seen from Fig. 19a that the misalignment shows negligible effects on the wheel load; Case 4, Case 5, and Case 6 show nearly identical fluctuation in the wheel loads. However, the misalignment significantly affects the wheel-rail lateral forces (Fig. 19b). The maximum lateral wheel-rail force in Case 5 occurs when the wheel passes a misalignment of 6.4 mm due to the misalignment-induced wheel-rail impact. The lateral wheel-rail force obtained in Case 4 and

Case 6 shows a similar tendency, and its maximum value is much lower than that in Case 5. Furthermore, the fluctuation amplitude of wheel-rail force in Case 6 is much lower than in Cases 4 and 5. Therefore, it can be concluded that, since the proposed device effectively eliminates the misalignment caused by the manufacturing variation of the FPB, the wheel-rail impact is significantly reduced.

The incremental dynamic analysis (IDA) is applied to the vehicle-bridge system for Case 5 and Case 6 to determine the effect of the proposed device on the vehicle's performance on bridges during an earthquake. The PGA of all the ground motion records was scaled from 0.1 g to 0.6 g with a step of 0.1 g. The train composed of 8 vehicles is assumed to run over the bridge at the speed of 200 km/h.

Figure 20 shows the IDA results of the wheel-rail forces with different constraint conditions. The wheel-rail forces show an increasing trend with PGA of the ground motion. In Fig. 20, it was found that the proposed misalignment control device (Case 6) can efficiently reduce the wheel-rail forces, especially for the lateral wheel-rail forces, compared to Case 5. The normal track can only moderately limit the misalignment, resulting in a significant misalignment-induced wheel-rail impact when the wheelsets pass over the girder end. In contrast, the proposed misalignment control device in Case 6 can effectively limit the misalignment and significantly reduce the wheel-rail impact.

It is difficult to obtain the statistical value of the maximum wheel-rail forces under the earthquakes since the misalignment obeys the non-gaussian distribution in Section 2. Therefore, it is recommended to install the proposed misalignment control device on railway bridges with FPBs to reduce the misalignment-induced wheel-rail impact. In the following comparisons and analysis, only Case 6 will be considered.

5.4 Effect of the FPB on the seismic response of the bridge

The vehicle-bridge responses are analyzed under different earthquake intensities based on the 50-span simply supported bridge established in the previous subsection. The stiffness of the non-isolated bearing, i.e., spherical steel bearing, is as follows: 7.5e5kN/m in the longitudinal and lateral direction, and 6.4e6kN/m in the vertical direction, respectively. The bridge's natural frequencies of the lateral and vertical modes with non-isolated bearing are 2.58 Hz and 4.47 Hz, respectively.

The vehicle-bridge responses were analyzed using the model in Fig. 16, shaken by the 11 seismic records. In this simulation, the train composed of 8 vehicles is assumed to run over the bridge at the speed of 200 km/h. The ground motion is assumed to start when the first vehicle reaches the 8th span of the bridge, making the train on the bridge when the peak acceleration attacks the bridge. In addition, the traveling wave effects are not considered in this study.

Figure 21 shows the relative lateral displacement and the acceleration of the 25th span bridge deck with a running vehicle on the bridge excited by the No.1 ground motion with a PGA of 0.2 g. As seen from the figure, compared with the non-isolation bearings, the FPBs increase the girder's lateral displacement but reduce its lateral acceleration after the shear pin is cut off. This effect is expected since the FPB reduced the lateral stiffness and prolonged the vibration period of the bridge.

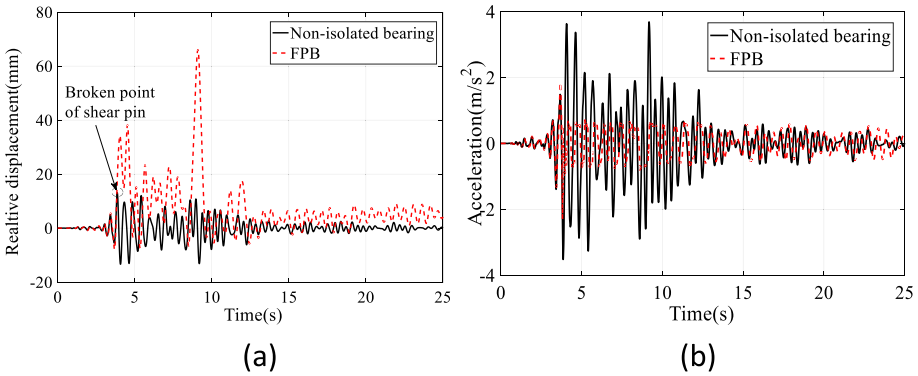

Fig. 21 Response of bridge deck undergoing No.1 ground motion: **a** relative displacement of the bridge deck; and **b** acceleration of the bridge deck

The incremental dynamic analysis (IDA) procedure is applied to the vehicle-bridge system to show the effect of FPB on the bridge's response under different seismic intensities. In the IDA analysis, the PGA of the ground motion records was scaled from 0.1 g to 0.6 g with a step of 0.1 g.

Figure 22 shows the IDA analysis results of the bridge's seismic response subjected to different earthquake intensities. The solid line denotes the bridge with FPBs; the dashed line denotes the bridge with non-isolated bearings. It is clear from Fig. 22 that the relative displacement between the bridge deck and pier top of non-isolated bridges is much larger than that of the isolated bridge. The reason is that the shear pins were cut off to isolated seismic energy under larger earthquakes. Thus, the moment at the pier bottom of the bridge with FPB is much smaller than those with non-isolated bearing.

5.5 Effect of the FPB on the seismic safety of the vehicle

Figure 23 shows the vehicle's response on the bridge subjected to No.1 ground motion with a PGA of 0.2 g. It can be seen that the vehicle response on the bridges with FPBs is smaller than those on the bridge with non-isolated bearings. The reason is that the FPB effectively reduces the bridge deck's acceleration and vehicle-track system's input.

Figure 24 shows the IDA analysis results of vehicle's responses subjected to different earthquake intensities. The solid line denotes the vehicle response on the bridge with FPBs; the dashed line denotes the vehicle responses on the bridge with non-isolated bearings. It is clear from Fig. 24 that the accelerations of the car body show an increasing trend with the PGA of the ground motion. Also, there is no significant difference between the FPB and the non-isolated bearing when the PGA is less than 0.1 g because the shear pin is required to provide enough shear strength to remain intact at a small earthquake (typically for PGA < 0.1 g) (Jiang et al. 2019). However, the shear pins were cut off to isolated seismic energy under larger earthquakes. Thus, the vehicle's responses on bridges with FPBs are much smaller than those with non-isolated bearing.

Figure 24b shows the wheel unloading rate and derailment coefficient directly related to running safety. In Japanese Code (RTRI-Displacement Limits 2006), the design limit values of wheel unloading rate and derailment coefficient are 0.8. The vehicle's wheel unloading rate and derailment coefficient on the non-isolated bridge will exceed the limit values when the PGA is larger than 0.3 g. However, the vehicle's wheel unloading

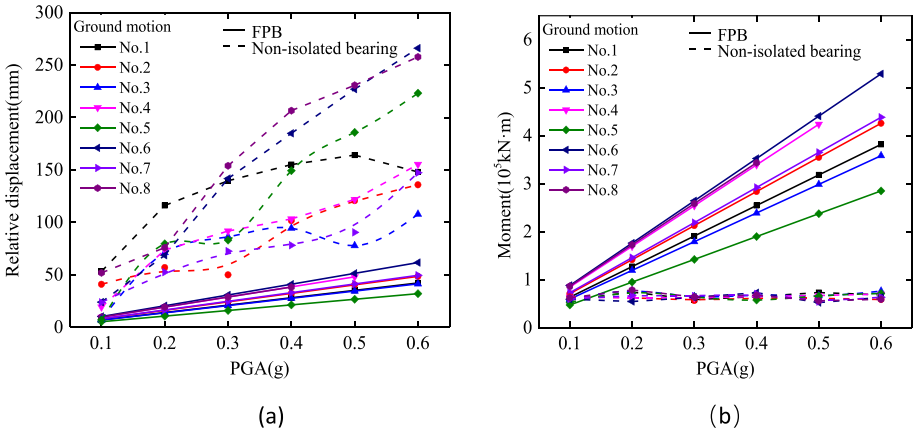

Fig. 22 IDA results of the bridge response: **a** relative displacement of the bridge deck; and **b** moment at pier bottom

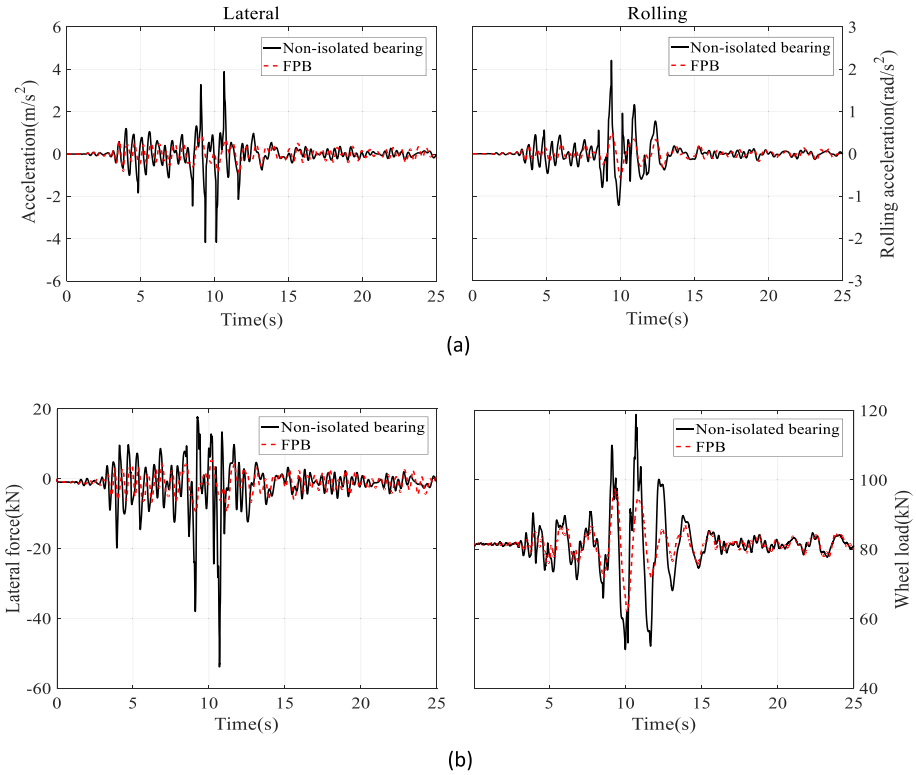

Fig. 23 Responses of the vehicle undergoing No.1 ground motion: **a** car-body; and **b** wheel-rail forces

rate and derailment coefficient on the bridge equipped with FPB are generally less than the limit values for all ground motion records, indicating that the FPB can provide higher running safety against an earthquake.

Figure 24c shows the wheel-rail displacement directly related to derailment assessment. The vertical wheel-rail displacement reaches 28 mm, and lateral wheel-rail displacement reaches 94 mm is defined as two derailment criteria (Jin and Pei 2016). In this study, the vertical wheel-rail displacement reaching 28 mm is selected as the derailment

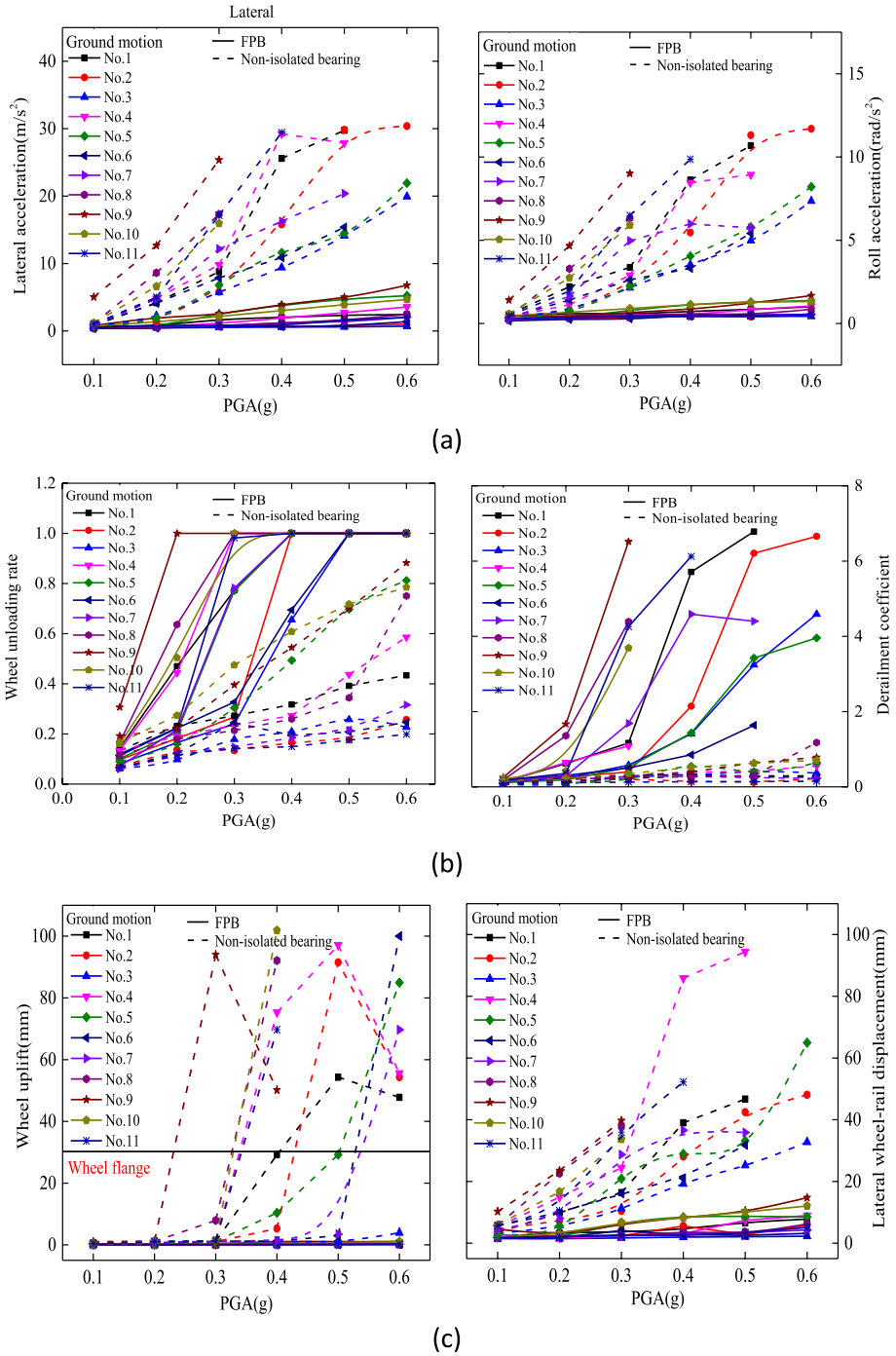

Fig. 24 IDA results of the dynamic response of the vehicle: **a** car-body's acceleration; **b** assessment indices; and **c** wheel-rail relative displacement

criteria. Based on these criteria, the vehicle derailed in ten among the eleven ground motion records when the vehicle was running on the non-isolated bridge. In contrast, no derailment occurred on the bridge equipped with FPB and the misalignment control device for all ground motion records. Therefore, it can be concluded that the FPB with

the misalignment control device can improve the running safety of the vehicles on the bridge during an earthquake.

6 Summary

In this study, the full nonlinear model of the FPB model was introduced into the vehicle-track-bridge interaction model to investigate the vehicle's performance under earthquakes. The effect of the misalignment caused by the manufacturing variation of FPB on the wheel-rail forces was investigated. A device was proposed to reduce the misalignment-induced wheel-rail impact. Finally, the responses of the vehicles on isolated bridges with FPBs are comprehensively compared with those of non-isolated bearing. From the simulated results through the bridge structure and parameters used in this study, the main conclusions are as follows:

(1) For bridges equipped with FPB, a large lateral misalignment may occur at girder ends when considering the manufacturing variation of FPB (i.e., shear pin's strength and friction coefficient). When the friction coefficient of the FPB is assumed as Gaussian distribution, the misalignment is an asymmetric bimodal distribution. In addition, the misalignment at the girder end is very irregular for the Gaussian distribution of the shear pin's strength.
(2) The full nonlinear behavior of FPB is introduced into the vehicle-bridge interaction model. Using this model, the lateral misalignments at girder ends caused by the manufacturing variation of FPB significantly increased the wheel-rail lateral force.
(3) A misalignment control device was proposed to limit the misalignment on the isolated bridge with FPBs. The vehicle-bridge simulation found that the proposed device can effectively reduce the wheel-rail forces, especially for the lateral wheel-rail force. The FPB with the misalignment control device can significantly reduce the wheel-rail uplift, making it possible to achieve a derailment-free design for bridges under strong earthquakes.

Acknowledgements
Not applicable.

Authors' contributions
Zhibin Jin: Conceptualization, Methodology, Supervision, Writing-review & editing. Ke Chen: Investigation, Data analysis, Writing-original draft. Jinzhe He: Software, Validation. All authors have read and approved the manuscript.

Funding
This study is supported by the National Natural Science Foundation of China (Grant No. 51678490); the National Science Fund for Distinguished Young Scholars (51525804); and China-Indonesia Joint Research Center for High-speed Railway Technology (Grant No. KY201801005).

Availability of data and materials
Some or all data, models, or code generated or used during the study are available from the corresponding author by request.

Declarations

Competing interests
The authors declare that they have no competing interests.

Received: 13 April 2022 Accepted: 9 June 2022
Published online: 29 June 2022

References

American Society of Civil Engineers (2016) Minimum design loads for building and other structures. Draft version of Standard ASCE/SEI 7–16.
Bin Y, Shi L, Gonglian D et al (2016) Nonlinear interaction between CRTS II ballasteless track and bridges due to multi-dimensional earthquake. J China Railw Soc 38(5):74–80 (In Chinese)
Chamorro R, Escalona JL, Recuero AM (2014) Stability analysis of multibody systems with long flexible bodies using the moving modes method and its application to railroad dynamics. J Comput Nonlinear Dyn 9(1):011005
Chen LK, Jiang LZ, Qin HX et al (2019a) Nonlinear seismic assessment of isolated high-speed railway bridge subjected to near-fault earthquake scenarios. Struct Infrastruct Eng 15(11):1529–1547
Chen Z, Han Z, Zhai W et al (2019b) TMD design for seismic vibration control of high-pier bridges in Sichuan-Tibet Railway and its influence on running trains. Veh Syst Dyn 57(2):207–225
Eröz M, DesRoches R (2013) The influence of design parameters on the response of bridges seismically isolated with the Friction Pendulum System (FPS). Eng Struct 56:585–599
Federal Emergency Management Agency (2009) Quantification of building seismic performance factors: FEMA P695. Federal Emergency Management Agency, Washington DC
Fenz DM, Constantinou MC (2006) Behaviour of the double concave friction pendulum bearing. Earthq Engng Struct Dyn 35:1403–1424
Guo W, Du Q, Huang Z et al (2020) An improved equivalent energy-based design procedure for seismic isolation system of simply supported bridge in China's high-speed railway. Soil Dyn Earthq Eng 134:106161
Hassan AL, Billah AM (2020) Influence of ground motion duration and isolation bearings on the seismic response of base-isolated bridges. Eng Struct 222:111129
He W, Jiang L, Wei B et al (2020) The influence of pier height on the seismic isolation effectiveness of friction pendulum bearing for Double-Track railway bridges. Structures 28:1870–1884
Japan Transport Safety Board (2017) Railway accident investigation report train derailment. RA2017-8-II
Jiang L, He W, Wei B et al (2019) The shear pin strength of friction pendulum bearings (FPB) in simply supported railway bridges. Bull Earthq Eng 17:6109–6139
Jin Z, Pei S et al (2016) Effect of vertical ground motion on earthquake-induced derailment of railway vehicles over simply-supported bridges. J Sound Vib 383(24):277–294
Jin Z, Hu C, Pei S, Liu H (2018) An integrated explicit–implicit algorithm for vehicle–rail–bridge dynamic simulations. Proc Inst Mech Eng F J Rail Rapid Transit 232(6):1895–1913
Luo X (2021) Seismic running safety of trains and a new type of seismic-isolation railway structure. Transp Saf Environ 3(2):152–165
Madhekar SN, Jangid RS (2010) Seismic performance of benchmark highway bridge with variable friction pendulum system. Adv Struct Eng 13(4):561–589
Mitoulis SA (2012) The inefficacy of seismic isolation in bridges with tall piers. In: Proceedings of 15th World Conference on Earthquake Engineering, Lisbon, Portugal
RTRI-Displacement Limits (2006) Design standards for railway structures and commentary (displacement limits). Railway Technical Research Institute, Tokyo
Shen ZY, Hedrick JK, Elkins JA (1983) A comparison of alternative creep force models for rail vehicle dynamic analysis. Veh Syst Dyn 12(1–3):79–83
Sogabe M, Ikeda M, Yanagisawa Y (2007) Train-running quality during earthquakes and its improvement for railway long span bridges. Q Rep RTRI 48(3):183–189
Tsopelas P, Constantinou MC, Kim YS, Okamoto S (1996) Experimental study of FPS system in bridge seismic isolation. Earthq Eng Struct Dyn 25(1):65–78
Yoshida K, Maeda M, Achiha H et al (2010) Improvement of running safety at earthquake on railway viaducts retrofitted with braces. J Struct Eng A 56:543–553 (in Japanese)
Yu Z, Li H, Wei B, Jiang L, Mao J (2018) Numerical analysis on longitudinal seismic responses of high-speed railway bridges isolated by friction pendulum bearings. J Vibroeng 20(4):1748–60
Zhai W (2020) Vehicle-track coupled dynamics: theory and application. Springer, Singapore
Zhai W, Xia H, Cai C et al (2013) High-speed train–track–bridge dynamic interactions–part I: theoretical model and numerical simulation. Int J Rail Transp 1(1–2):3–24

Publisher's Note